Applying analytical ultracentrifugation to nanocrystal suspensions

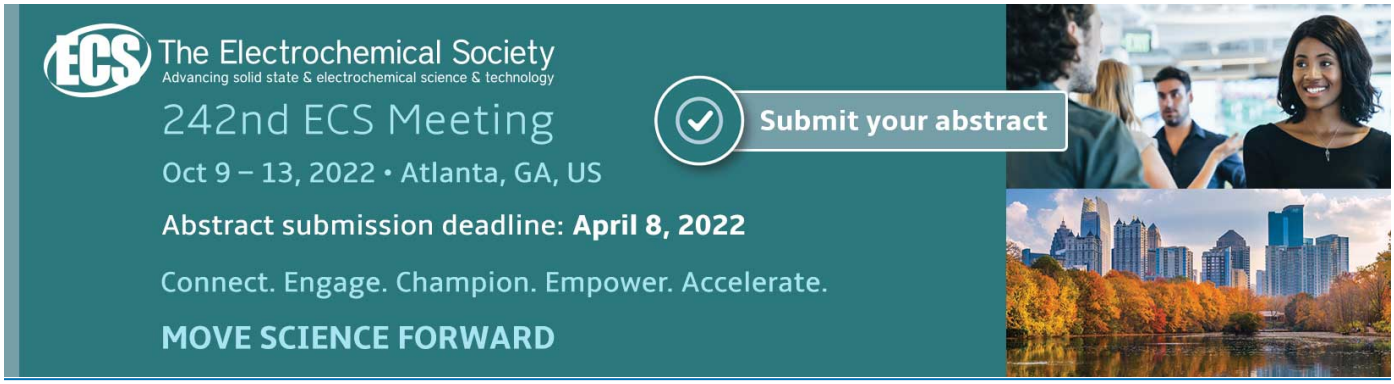

Nanotechnology **20** (2009) 355702 (10pp) doi:10.1088/0957-4484/20/35/355702

Applying analytical ultracentrifugation to nanocrystal suspensions

Jennifer A Jamison, Karl M Krueger, J T Mayo, Cafer T Yavuz, Jacina J Redden and Vicki L Colvin[1]

Department of Chemistry, Rice University, 6100 Main Street, MS-60, Houston, TX 77005, USA

E-mail: colvin@rice.edu

Received 14 November 2008, in final form 13 June 2009
Published 12 August 2009
Online at stacks.iop.org/Nano/20/355702

Abstract

While applied frequently in physical biochemistry to the study of protein complexes, the quantitative use of analytical ultracentrifugation (AUC) for nanocrystal analysis is relatively rare. Its application in nanoscience is potentially very powerful as it provides a measure of nanocrystal density, size and structure directly in the solution phase. Towards that end, this paper examines the best practices for applying data collection and analysis methods for AUC, geared towards the study of biomolecules, to the unique problems of nanoparticle analysis. Using uniform nanocrystals of cadmium selenide, we compared several schemes for analyzing raw sedimentation data. Comparable values of the mean sedimentation coefficients (s-value) were found using several popular analytical approaches; however, the distribution in sample s-values is best captured using the van Holde–Weischt algorithm. Measured s-values could be reproducibly collected if sample temperature and concentration were controlled; under these circumstances, the variability for average sedimentation values was typically 5%. The full shape of the distribution in s-values, however, is not easily subjected to quantitative interpretation. Moreover, the selection of the appropriate sedimentation speed is crucial for AUC of nanocrystals as the density of inorganic nanocrystals is much larger than that of solvents. Quantitative analysis of sedimentation properties will allow for better agreement between experimental and theoretical models of nanocrystal solution behavior, as well as providing deeper insight into the hydrodynamic size and solution properties of nanomaterials.

S Supplementary data are available from stacks.iop.org/Nano/20/355702

(Some figures in this article are in colour only in the electronic version)

1. Introduction

Analytical ultracentrifugation (AUC) measures the sedimentation properties of materials as they are settling in a centrifuge. Quantitative analysis of these data can yield a wealth of insights into the solution phase properties of nanoparticles since sedimentation speed depends sensitively on a material's hydrodynamic size, shape and density. As compared to dynamic light scattering, AUC offers a lower limit of detection and a greater sensitivity to changes in material density; moreover, unlike electrophoresis it is non-destructive and can be applied to nanoparticles suspended in virtually any solvent [1]. Over the past ten years, the application of AUC to nanomaterial analysis has been growing substantially; examples of its application can be found for a variety of systems including nanoscale TiO_2, Fe_3O_4, CdS, $ZrSO_4$, FePt, various other inorganic nanoparticles, carbon nanotubes, and a large variety of protein and polymeric nanoparticles [2–40]. More importantly, because AUC resolves solution species with angstrom sensitivity it is highly sensitive to the structure of nanoparticle surface coatings and the extent of their bioconjugation [1, 13–15, 38, 39, 41].

One of the first applications of analytical ultracentrifugation was to gold colloids almost a hundred years ago; however, its application in modern nanoscience has been relatively limited [42]. As a result best practices for collecting and analyzing nanocrystal sedimentation data are not well

[1] Author to whom any correspondence should be addressed.

defined. Much of the guidance for this method is directed towards the biochemistry community which uses AUC to evaluate and quantify protein–protein interactions. In principle the application of analytical ultracentrifugation to the analysis of nanoparticles does not require substantially different methods or analysis. The simple models of sedimenting spheres that guide the analysis of ultracentrifugation data are independent of sphere size. However, there are several issues that complicate experimental and quantitative analysis of nanocrystal sedimentation. Unlike some highly purified and uniform proteins, nanocrystals have intrinsic size and shape distributions which contribute to the breadth of sedimentation fronts. In addition, their sizable and wide ranging densities—often much larger than the surrounding fluids—complicates the selection of appropriate sedimentation speeds. Finally, much of the potential value of AUC in nanoscience lies with its ability to quantitatively specify the how fast nanocrystals sediment (e.g. the s-value). For adequate interpretation of such data, it is vital to assess the reproducibility and experimental error of AUC measurements on model nanocrystal samples.

In this work we show that the nanocrystal sedimentation coefficients, or s-values, can be both measured and analyzed using AUC techniques that are comparable to those developed for biomolecules. While many data analysis procedures can provide accurate measure of the average s-value of a nanocrystal sample, the van Holde–Weischet algorithm is best suited to describing the distribution of s-values. This model-independent approach explicitly addresses diffusion effects and can disentangle the breadth introduced from particle diffusion from that introduced by heterogeneous size and densities. We also identify experimental conditions that cause significant and erroneous variation in the overall sedimentation coefficient and corresponding distribution. Finally, we evaluate the sensitivity of AUC to conditions of particular importance to nanomaterials, such as the wavelength of detection and sedimentation speed.

2. Materials and methods

2.1. CdSe nanoparticle synthesis

The synthesis of CdSe nanocrystals was performed following a protocol similar to that of Yu *et al* [43]. Briefly, 0.51 g CdO (99.99% Aldrich), 3.76 g oleic acid (tech grade, Aldrich), and 160 ml of 1-octadecene (tech grade, Aldrich) were combined in a reaction flask in an air-free environment and the temperature was increased to 300 °C. Once the CdO mixture became colorless, a solution of 0.16 g Se (99.5%, Aldrich), 0.8 g TOP (tech grade, Aldrich) and 5 ml of ODE was injected using a syringe. A volume of 70 ml of ODE was added to quench the reaction. The reaction mixture was purified by adding acetone, centrifuging at 3200 rpm, and preserving the decantate. The decantate was further purified by the addition of acetone, followed by centrifuging at 3200 rpm and preserving the precipitate. Precipitates were resuspended in toluene (99.8%, Fischer), and the surfaces of the nanocrystals in suspension were stabilized by the addition of 30 μl of 1-dodecane thiol (98%, Aldrich) [44]. The concentration of the suspensions was estimated based on their optical absorbance in a standard 1 cm path length cuvette within a Varian Cary UV–visible spectrophotometer, and an absorption coefficient of 2×10^5 cm^{-1} M^{-1} for CdSe nanocrystals from [45].

2.2. Iron oxide nanoparticle synthesis

Ferroxyhydrate (gamma-FeOOH, 30–50 mesh, Aldrich) was finely crushed and dissolved in oleic acid (tech grade, Aldrich) in an air-free environment. This mixture was then diluted using 1-octadecene and allowed to reflux for 1 h. The resulting slurry was purified using a combination of acetone and hexane, and Fe_3O_4 nanocrystals were recovered in hexane [46].

2.3. Transmission electron microscopy and particle sizing

Images were obtained using a 100 kV JEOL TEM (JEM-2010). Small volumes of the nanocrystal suspensions were added to the surface of 300 mesh carbon/formvar coated copper grids (Ted Pella #01821) and allowed to evaporate in air. Particles were sized manually using ImagePro® software. TEM images and sizing histograms of CdSe and Fe_3O_4 are displayed in figures S1 and S2 respectively within the supplemental information (available at stacks.iop.org/Nano/20/355702).

2.4. Analytical ultracentrifugation

Sedimentation velocity experiments were performed on a Beckman Optima XL-A Ultracentrifuge. All data were obtained by monitoring the absorbance at 25 °C for 100 scans, except where otherwise indicated. Experimental set-up included aluminum centerpieces in the sample cells, which were centrifuged in an AnTi-60 rotor. All data were analyzed with Ultrascan 7.1 (enhanced van Holde–Weischet), employing at least 80% of the boundary region and a smoothing factor of less than 10 for all datasets. For typical operating conditions, we found that the results of AUC are reproducible and place conservative error bars of 5% on measured sedimentation coefficients. Less reliable were measurements of the properties at the wings of the distribution, therefore we estimated error bars of 20%. A sample data set was also analyzed using $c(s)$ (Ultrascan 7.1), ls-$g^*(s)$ (SEDFIT), and a manual determination.

The $c(s)$ analysis, or continuous distribution of sedimentation coefficients, is one of several solutions to the Lamm equation. In this analysis, the sedimentation coefficient is first determined from solving the Lamm equation. Then using an estimated frictional coefficient, solvent and solute densities, and solvent viscosity, the molecular weight of the solute is determined and subsequently used to calculate the diffusion coefficient according to equation (1):

$$D(s) = \frac{\sqrt{2}}{18\pi} kT s^{-\frac{1}{2}} (\eta (f/f_o)_w)^{-\frac{3}{2}} \times \left(\left(1 - \frac{\rho_{\text{solvent}}}{\rho_{\text{particle}}} \right) \rho_{\text{particle}} \right)^{\frac{1}{2}} \quad [47] \tag{1}$$

where D is the diffusion coefficient, k is Boltzmann's constant, T is temperature, s is the sedimentation coefficient, and ρ is density, η is viscosity. f_o is the frictional coefficient for

a perfect sphere, and is equal to $6\pi\eta r$ (η and r are solvent viscosity and hydrodynamic radius, respectively). In this equation, f/f_o is equal to 1. For a solute that is not a sphere, f/f_o is a number greater than 1. More extensive discussion of this analysis procedure is available elsewhere [47].

The ls-$g^*(s)$ analysis, or least-squares boundary modeling, mathematically compares the sedimentation profiles of the actual solutes with the sedimentation profiles of equivalent solutes that are free from the influence of diffusion via equation (2):

$$c(r,t) = \int g^*(s)U(s,r,t)\,\mathrm{d}s \qquad [48] \qquad (2)$$

with $c(r,t)$ representing the actual sedimentation of solutes and $U(s,r,t)$ representing diffusion-free sedimentation of the solutes and is defined as:

$$U(s,r,t) = \mathrm{e}^{-2\omega^2 st} \times \begin{cases} 0 & \text{for } r < r_\mathrm{m}\mathrm{e}^{\omega^w st} \\ 1 & \text{else} \end{cases} \qquad [48] \qquad (3)$$

where s is the sedimentation coefficient, ω is the angular velocity, t is time, r is radial position at time t, and r_m is the radial position at the meniscus. The solution to this integral equation is solved by a combination of discretization and application of a least-squares approximation, which allows simplification of equation (2) into:

$$\min_{g^*i} \sum_r \sum_t \left[c(r,t) - \sum_{s_\mathrm{min}}^{s_\mathrm{max}} g_i^* U(s_i,r,t)\Delta s \right]^2 \qquad [48] \quad (4)$$

which permits simple conversion of the data into the more familiar distribution of sedimentation coefficients. Detailed discussions of this analysis have been undertaken by Schuck and Rossmanith [48]. For application of ls-$g^*(s)$ to our data, we used s_min, s_max, and resolution values of 1, 100, and 100, respectively. The Tikhonov–Phillips regularization (default setting) was also employed.

The manual determination was undertaken as follows. The corresponding positions at 50% of the boundary for the first ten scans were evaluated using equation (5), as defined by Svedberg:

$$s = \ln\left(\frac{r_\mathrm{b}}{r_\mathrm{m}}\right)[\omega^2(t_\mathrm{b} - t_\mathrm{m})]^{-1} \qquad [42] \qquad (5)$$

where s is the sedimentation coefficient, r_b is the value of the radius at the boundary, r_m is the value of the radius at the meniscus, ω is the angular velocity, t_b and t_m are the times, in seconds, at radius positions r_b and r_m, respectively [42]. The average of the ten s-values was assumed to be the actual s-value of the data set. Sedimentation coefficients are reported to three significant figures because both the radial positions and densities of most solvents, which are used to analyze raw AUC data in some cases, are known accurately to three significant figures.

3. Results and discussion

The sedimentation coefficient of a material is the fundamental parameter for characterizing how it responds to gravitational or centrifugal forces. It can be conceptualized as the propensity of a material to move given a fixed force; materials with larger sedimentation coefficients move greater distances than those with smaller coefficients assuming all other factors are constant. To assess the sedimentation coefficient precisely, experimentalists measure the visual boundary of a material as it deposits over time. Over eighty years ago, Svedberg defined its form in equation (5) [42]. AUC is a technique which applies equation (5) to the evaluation of sedimentation directly in a centrifuge while it is occurring.

In a typical AUC experiment samples are placed in a specially designed centrifuge equipped with an optical spectrometer. The sample cells, which are typically 1.2 cm in length, contain sample volumes on the order of 500 μl; the cells are continually scanned during sedimentation and the solute is detected via optical density at a specified wavelength. When the rotor is spinning, materials will experience substantial sedimentation forces and move away from the center of the apparatus towards the bottom of the cell. The homogeneous optical density of the suspensions will thus change accordingly, and with time lower optical density will be measured at the top of the cell as sample is depleted due to sedimentation.

Figure 1(A) shows typical raw data collected for a representative sample of nanocrystalline cadmium selenide in toluene. The curves have an s-shape with low optical density towards the 'top' of the cell and higher values measured at the bottom. With increasing time the boundary of the curves (defined as the midpoint between the zero optical density top and the higher concentration bottom) shifts away from the center as the materials sediment into pellets. The red curve corresponds to the sedimentation front at an earlier time in the experiment than the green curve; typically tens to hundreds of sedimentation fronts are collected over the course of a several hour experiment.

Also apparent in figure 1(A) is that the transition from the highly concentrated region at the cell bottom and the sedimenting species at the top is not as sharp; the sedimentation front is spread spatially in the cell. A perfectly homogeneous sample with only one sedimentation coefficient would, in principle, present a sedimentation profile which was a step function. As it is, heterogeneity in both the sample and particle diffusion broaden the sedimentation boundary. In order to more realistically model sedimentation, and thereby extract quantitative data from these raw datasets, any one of several sophisticated data analysis packages can be employed. These process the raw data by fitting the sedimentation profiles in time so as to yield an average s-value for the sample as well as a measure of the distribution in the s-values due to sample heterogeneity.

While there are several approaches to analyzing raw sedimentation of the type shown in figure 1(A), the van Holde–Weischet analysis provides a strategy which has few underlying assumptions and is well suited to nanoparticle

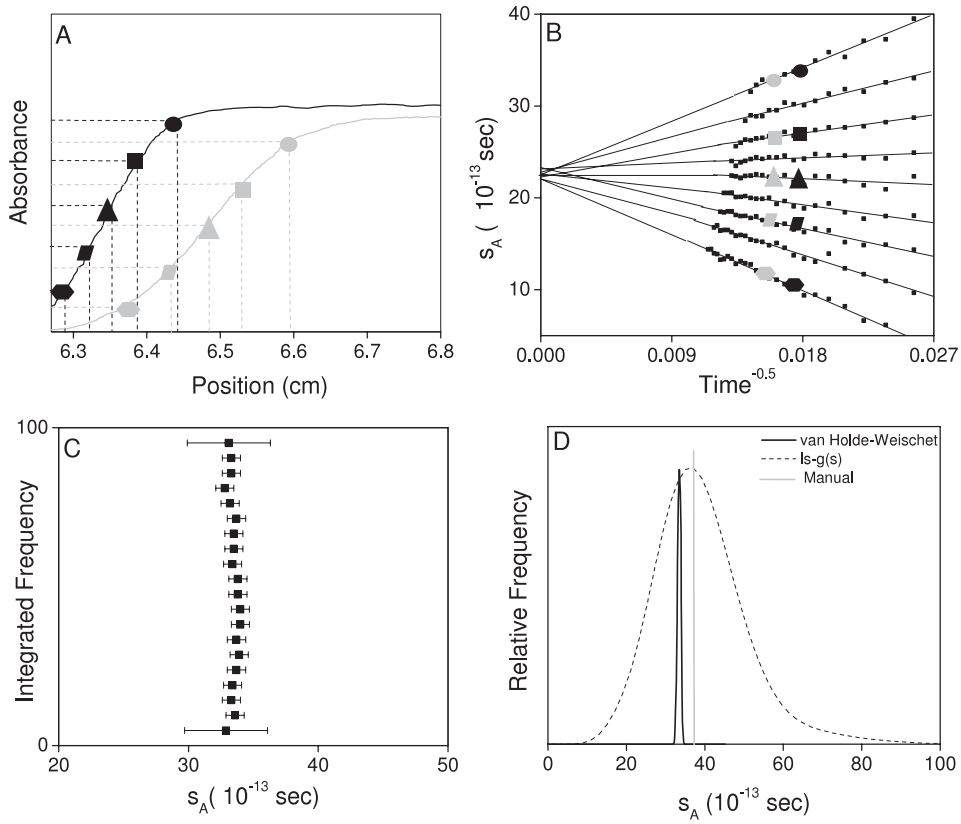

Figure 1. Illustration of the van Holde–Weischet analysis and comparison of most common analysis methods for a model sample of 3.1 nm in diameter CdSe nanocrystals. (A) Sedimentation curves are collected at distinct time points, shown here as black and gray. Each curve in the sedimentation profile is then divided into equal fractions along the y-axis and the values of the corresponding positions along the x-axis for each fraction are evaluated by equation (1). (B) A plot of equation (1) (s-value versus time$^{-0.5}$). The convergence of the lines at the y-axis indicates the s-value of the sample. (C) Integral plot of s-values. Each line from (B) has a fractional value assigned to it that corresponds to integrated frequency values ranging from 0 to 100. (D) Histogram plots of s-values. The data from (B) can also be represented with a histogram. Also shown are s-value determinations using other types of analyses. In general, all methods yield similar s-values and the only difference lies in the width of the distributions.

systems. The $c(s)$ approach to AUC data analysis fits the raw data to a series of curves that are solutions to the Lamm equation; because of their larger size, nanoparticles may not obey the conventional models for molecular solutes at dilute conditions that underlie this treatment. The second category of data analysis is made up of model-independent approaches, such as the time-derivative and van Holde–Weischet analyses. This latter process is widely used in the analysis of biomolecular sedimentation and is well suited for capturing the behavior of systems that have significant heterogeneity [1, 47, 49, 50]. These methods rely on mathematical transformations of the raw data to facilitate the measure of the average sedimentation coefficient and its distribution. The assumptions underlying these data analysis techniques are relatively minor, and include the condition that diffusive motion is less significant than motion caused by sedimentation as well as the neglect of the finite cell length and sedimentation timescale. While its applicability to the analysis of nanoparticles of the smallest dimensions has been questioned [14], we show here that the van Holde–Weischet analysis is in fact appropriate for small inorganic nanocrystals that have densities differing greatly from their suspending solvents.

Figure 1 illustrates how the van Holde–Weischet analysis is applied to a dataset describing the sedimentation of CdSe nanocrystals. Sedimentation profiles at a single time are first sampled at discrete intervals defined by proscribed increments of optical density (figure 1(A), symbols). The equivalent s-values at those positions are then found using equation (1). Such an analysis is performed for all scans included in the dataset, resulting in sets of s-values found at different times (figure 1(A)). In order to discern the effect of diffusion from sample heterogeneity, the van Holde–Weischet analysis relies on the fact that diffusive time-dependent changes in the boundary will have a different dependence on time than broadening due to sample heterogeneity. Specifically, diffusion will grow with the square root of time and thus graphs of s-values versus $t^{-1/2}$ when extrapolated to infinitely long time provide a s-value average and distribution reflective of the sample heterogeneity [51, 52]. In figure 1(B) and the intercepts at the y-axis provide a measure of the sample's true sedimentation coefficient with no contribution from diffusion. These linear fits also introduce the greatest source of error into s-value determination for a given point in the distribution; the correlation coefficients of these fits help to constrain the error bars reported in figure 1(C).

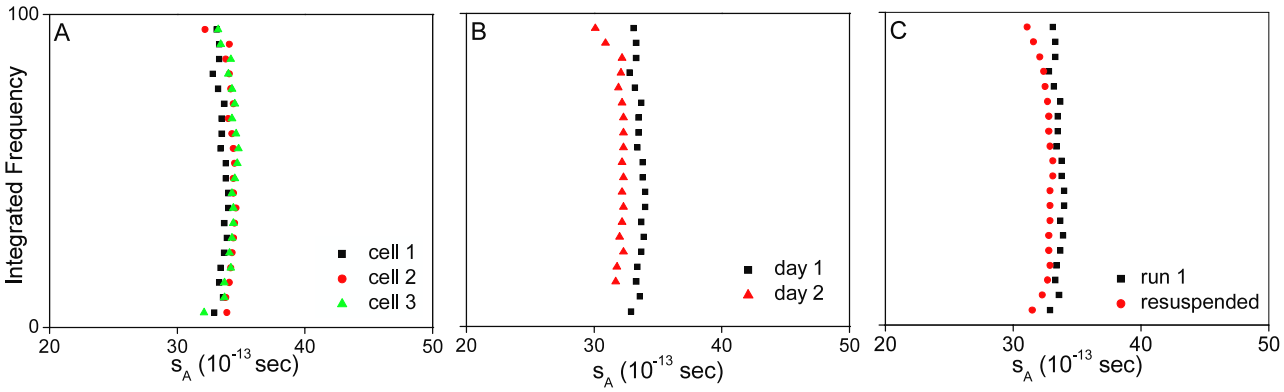

Figure 2. Reproducibility of analytical ultracentrifugation datasets. (A) The same sample, run in separate cells during the same experiment, gives nearly identical results. (B) Small variation is observed for different aliquots of the same sample run on different days. (C) A slight shift in s-value is also observed for the same sample aliquot run once, resuspended, and run a second time.

Such data can then be displayed in terms of a frequency profile (figure 1(C)) or as a more conventional s-value distribution (figure 1(D)). In this work we report the former as it does not emphasize the more error-prone wings of the distributions. The wings of the distribution are more difficult to specify as they are a less concentrated population within the sample, and thus provide lower optical densities for detection. The result of the van Holde–Weischet analysis is then a measure not only of the average s-value, but also its distribution. Additional information can also be extracted to describe more subtle details about attractive or repulsive interactions between the nanoparticles. A discussion of this is beyond the scope of this paper, and the reader is referred to more expansive treatments of the van Holde–Weischet analysis [52].

In order to examine the influence of the data analysis process on the measured sedimentation coefficient, the dataset used in figure 1 was also analyzed manually to provide a single average s-value as well as ls-$g^*(s)$. We obtained average sedimentation coefficients of 39.9 and 37.2 S, respectively. The average sedimentation coefficients derived from all the methods agree well with the value obtained by the van Holde–Weischet analysis (33 S). The s-value is largest when evaluated manually due to the fact that only the first ten scans of the data set were employed, while all other methods applied at least fifty scans.

Greater differences between the methods are found in their description of the breadth of the sedimentation curves. The van Holde–Weischet approach yielded the narrowest range of s-values (32–35 S), in good qualitative agreement with narrow core distributions that we found in TEM (figure S1 in supplemental information available at stacks.iop.org/Nano/20/355702). A more quantitative analysis of the distribution width, and its relationship to the core diameter distribution, requires an accurate model for nanoparticle density that incorporates realistic structures for the organic coatings [41]. However, one would expect for both material types that s-value distributions would range only over approximately 15 S based on accounting of the core distribution alone. In contrast to the narrow distribution derived from the van Holde–Weischet analysis, ls-$g^*(s)$ yielded a broader range of sedimentation coefficients and 9–92 S. These measured distributions were extremely sensitive to user-defined parameters, unlike the average reported for the distribution was generally unchanged. Examples of how these parameters, which include details about how the data is fit, affect the resulting datasets are given in the supplementary information (figure S3 and supplemental table 1—supplemental information available at stacks.iop.org/Nano/20/355702). The manual determination generated a relatively narrow range of s-values, spanning from 39–42 S, but we emphasize that only single points of a few scans were employed for calculation. In the interest of clarity and word count, we could not include all possible methods here. We note that the radial derivative and $c(s)$ methods (figure S4—supplemental information available at stacks.iop.org/Nano/20/355702) are comparable to the ls-$g^*(s)$ and other model-independent approaches in terms of obtaining the same average s-value. However, the $c(s)$ model is not suitable for observing the s-value distribution in this case because the corresponding residuals indicate that this analysis is a bad fit for this particular system. Further evaluation of these analysis methods are the subject of ongoing work.

In addition to data analysis, the reproducibility of the analytical ultracentrifuge is of great importance for its current and future applications. Run to run variability of average sedimentation coefficients from samples taken at different times and different days was on the order of 5%. However variability is much lower for samples run at the same time. An analytical ultracentrifuge fitted with an AnTi-60 rotor has the capability of collecting data on three samples per run, at the same speed and detection wavelength. Figure 2(A) illustrates that cell to cell variability in AUC analysis is minimal. The standard deviation in the average s-values (33.5, 34.1, and 34.1 S) obtained from all three cells in a single run is 0.36 S, or approximately 1.1% of the reported s-value. This is in contrast to run variability in samples that were taken from the same stock solution of nanoparticles and measured on different days (figure 2(B)). We note that the sample was visually stable over the time span between experimental runs. We would anticipate replicate measurement error of average s-value for

nanocrystals to be on the order of 5%, as illustrated in these data (34.1 and 32.5 S).

Finally, we show in figure 2(C) the variation in *s*-values for a single aliquot run twice. The sample was sedimented, subsequently resuspended, and then analyzed a second time. We were able to recover our samples and measure identical AUC data after sedimentation; this observation is not anomalous in our experience and is generally true for smaller nanocrystal samples with polymeric coatings. We note, however, that the recovery of samples should always be evaluated independently to rule out aggregation. Such sample recovery is not possible with proteins for example, and for some nanoparticle systems sedimentation could result in interparticle aggregation. However, in this case the coincidence of the sedimentation properties before and after suggest that at least for some samples the technique is non-destructive. The average *s*-values (32.2 and 32.4 S) calculated from both experiments are nearly identical, demonstrating that AUC is highly reproducible for coated nanomaterials. These results, in principle, are not surprising since sedimentation relies solely on the unique properties of all solution components. In addition, we also demonstrate that the ultracentrifugation process itself, even at very high speeds, does not in this example significantly alter the sample. Materials can be recovered for use in further applications. This result is in agreement with data shown previously for aqueous nanoparticles at much lower speeds [1].

Operational parameters such as temperature, sample concentration, rotor speed and detection wavelength can contribute to systematic variations in quantitative measurement of sedimentation properties. Because of the large density of inorganic nanoparticles the selection of appropriate rotor speeds is particularly crucial. In figure 3, we show that if the rotor speed is too slow then the measured sedimentation coefficient for a nanoparticle sample is dominated by artifact. For the sample of CdSe nanocrystals in figure 3, the average *s*-value of 32.6 S is well established experimentally and also in good agreement with theoretical expectations based on particle dimensions and density [41]. When the rotor speed was between 10 000 and 25 000 rpm, the average *s*-values agreed with this established value (figure 3(A)). However, at a rotor speed of 5100 rpm, the average *s*-value was spuriously large, 70 S, more than double its actual value. Figure 3(B) illustrates that this effect is not linear with speed but rather becomes significant only at a threshold below 10 000 rpm. At speeds of 10 000 rpm and greater, the corresponding integral plots are nearly vertical, indicating that the sample was comprised of a relatively narrow distribution of particles in good agreement with TEM data. Below 5100 rpm, however, not only is the *s*-value inflated, the distribution of *s*-values is very, very broad and ranges from 55 to 100 S.

These artifacts at slower rotor speeds arise because under these conditions nanoparticles sediment very slowly, so much so that diffusive broadening dominates the sedimentation front. The timescale of sedimentation increases substantially as the rotor speed is decreased; for example, sedimentation times at 10 000 rpm were 6 h and at 25 000 rpm the process was complete in just over 1 h (figure 3(C)). In contrast, complete

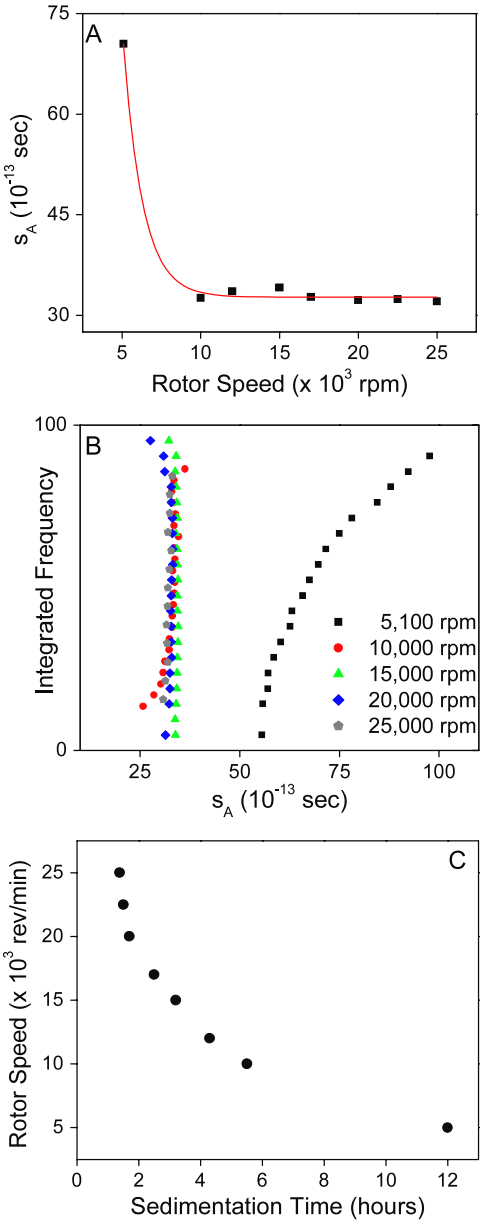

Figure 3. The effect of rotor speed on *s*-value and sedimentation time. Experiments were conducted on CdSe 52 with temperature and wavelength held constant at 25 °C and 541 nm, respectively. (A) A wide range of rotor speeds yield similar sedimentation coefficients. The 5 krpm speed yielded an erroneously larger average sedimentation coefficient due to diffusion effects becoming more pronounced at lower speeds. (B) The 5100 rpm speed also affected the sedimentation coefficient distribution, providing a much broader range of *s*-values that is not consistent with TEM characterization. (C) The sedimentation time increased drastically as rotor speed decreased.

sedimentation at 5000 rpm took 12 h. When sedimentation proceeds slowly for smaller particles, such as these CdSe nanocrystals, diffusion plays a significantly larger role in the overall transport process, effectively inflating the *s*-value.

These data thus establish the rather narrow conditions under which the van Holde–Weischet analysis is not appropriate: namely, when diffusion dominates the sedimentation profile. If samples must be evaluated at slower speeds for

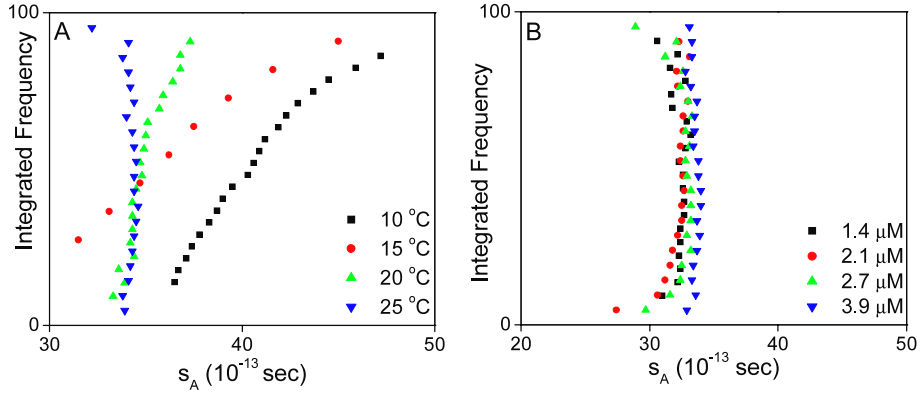

Figure 4. Dependence of sedimentation profiles on temperature and relative concentration. (A) Lower temperatures caused an increase in s-value and the s-value distribution for CdSe nanocrystals suspended in toluene, due to organic solvent properties being more sensitive to temperatures in this range than water. (B) Concentration did not significantly affect the average s-values and distributions.

some reason the $c(s)$ approach may be more accurate for absolute determination of s-values. Using this method we obtained s-values for 5100, 12 000, 17 000 and 25 000 rpm from 32 to 35 S, in good agreement with the value of the sedimentation coefficient in the absence of excessive diffusion. However, we must also note that the diffusion coefficients calculated under the $c(s)$ conditions are similar for speeds of 10 000 rpm and greater (approximately 1.2×10^{-7} m^2 s^{-1}), whereas the diffusion coefficient is estimated to be 1.5×10^{-7} m^2 s^{-1} for the 5100 rpm case. Although the differences in diffusion coefficients may not seem large, the effects are much more noticeable at the slower rotor speed because sedimentation is proceeding more slowly. Though a relatively wide range of speeds yields reasonable sedimentation profiles for nanocrystals, ideally these materials should be evaluated at sufficiently high speeds so as to minimize diffusion. However, if samples sediment too quickly to permit adequate collection of scans (at least fifty) for analysis then other sources of error enter into the analysis process. It is our best recommendation that several appropriate speeds on one sample be run in order to ensure ideal sedimentation conditions have been achieved.

Temperature and sample concentration also affect the sedimentation of nanoparticles. The effects of these variables have been well-documented in traditional AUC of biomolecules and polymers [53–59], and more recently, colloids and nanoparticles [31, 32, 37, 60–64]. These studies have generally shown that the sedimentation coefficient increases with increasing temperature due to polymerization or aggregation of the solutes [53, 56]. Additionally, viscosity is a parameter that is highly sensitive to temperature, and also effects sedimentation. Most modern analytical ultracentrifugation systems are equipped with thermal control accurate to ± 1 °C for this reason and thus this parameter contributes little to the operational error. Furthermore, the Ultrascan analysis program accounts for the effect of temperature on viscosity, thereby allowing for the most accurate determination of the sedimentation coefficient. Figure 4(A) shows the impact of temperature on the s-value and distribution of s-values. For our model CdSe nanocrystals suspended in toluene and run at the same speed, we have determined the average s-value to be approximately 33 S with a very narrow range (33–34 S) at 25 °C. The average s-value increased to 35.1 S at 20 °C and the range of s-values spanned from 34–36 S.

At temperatures of 10 and 15 °C the average s-values do increase, and exceed the 5% run to run variability expected for an AUC experiment. The 10 and 15 °C experiments yielded average s-values of 40.8 S and 37.4 S, respectively. In general, we note an increase in s-value for each decrease in temperature. A similar effect has also been observed in RNA sedimentation studies which attributed the phenomenon to changes in molecular conformation from a coil at lower temperatures to more extended at higher temperatures [65]. A more noticeable effect at 10 and 15 °C, however, is that the range of s-values is markedly broader than the 20 and 25 °C experiments: 32–45 S and 36–48 S, respectively. We attribute this to decreased solubility of the nanoparticles and possible aggregation of the nanocrystals at lower temperatures [66, 67].

In general, sedimentation coefficients linearly decrease with increasing concentration because the overall solution viscosity corresponds to the amount of solute present [32, 37, 58, 62, 64]. In figure 4(B), we show the dependence of sedimentation coefficient on concentration. For nanoparticle concentrations ranging from 1.4 to 3.9 μM, we observed no significant change in the average s-value. All of these values are within the experimental error of the experiment. Interestingly, however, the highest concentration yielded a slightly larger s-value (34.1 S) than the other concentrations, indicating that aggregation may have started to occur.

A final experimental parameter that we have found to be of particular importance to sedimentation analysis of nanocrystals is the detection wavelength. Figure 5 shows how the sedimentation coefficient distribution for CdSe and Fe_3O_4 nanocrystals changes as different detection wavelengths are selected. In figure 5(A), detection wavelengths of 432 and 541 nm both yielded average sedimentation coefficients of approximately 33 S for CdSe nanocrystals. However, a broader distribution was observed when samples were monitored at 432 nm as compared to 541 nm. This can be explained by the fact after the initial exciton peak at 541, excitations to the higher excited states create a continuum the makes for strong

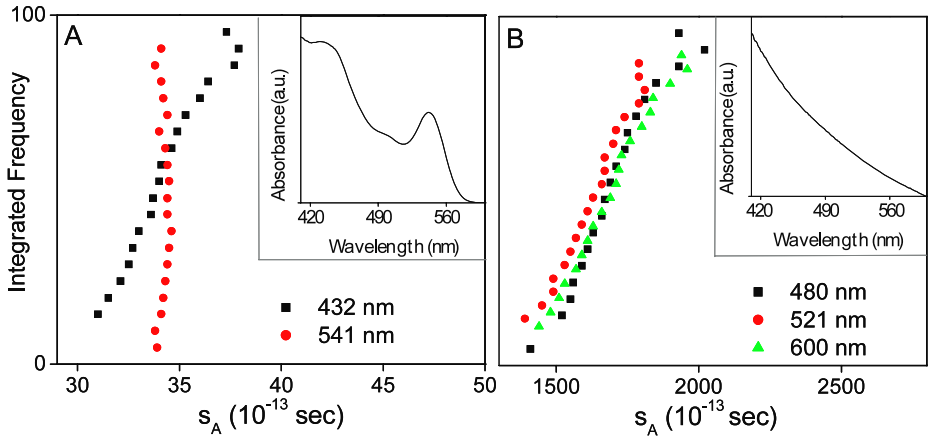

Figure 5. The effect of monitoring wavelength on CdSe and Fe_3O_4 nanocrystals. (A) CdSe nanocrystals, which have size-dependent absorption characteristics, yielded the same average sedimentation coefficient for two different wavelengths; however, the range of *s*-values is broadened at the lower wavelength. (B) Fe_3O_4 nanocrystals showed no variation in the range of *s*-values obtained for multiple wavelengths.

and relatively size-independent absorption. Thus the 432 nm detection wavelength is in effect sampling the entire population even those quantum dots that are very small and difficult to image via TEM. In contrast, the choice of a 541 nm detection wavelength makes for the most sensitive measurement as it is at a maximum optical density well known to correspond to quantum dots. For these samples, assuming a homogeneous linewidth of roughly 10 nm and a core distribution of 15% from TEM analysis, we can estimate that 80% of the sample mass is absorbing at this wavelength. Thus by comparing different optical detection wavelengths, it is possible to reveal smaller populations of quantum dots—difficult to image via TEM—yet still contributing to the overall absorption spectrum. In contrast, figure 5(B) shows the wavelength of detection has little effect on data from Fe_3O_4 nanocrystals which do not show size-dependent optical absorption. We compared three different wavelengths and obtained the same average *s*-value (∼1700 S) and distribution in all cases.

4. Conclusions

In conclusion, analytical ultracentrifugation can be applied to nanocrystal suspensions. Although data analysis methods do not typically affect average *s*-values, the distribution of *s*-values is generally widest for those that are model-dependent and/or do not correct for diffusion. The van Holde–Weischet analysis provides an effective way to account for both diffusion broadening as well as sample heterogeneity in AUC datasets. The resulting datasets describe both the average sedimentation coefficient as well as the distribution of sedimentation coefficients for a nanocrystal sample. Typical run to run variability in a conventional analytical ultracentrifugation instrument is low, not more than 5%, in reported sedimentation coefficient average and distribution width. Operational factors such as temperature and material concentration have minor effects on measured data, most of which are accounted for in the analysis process. Some nanocrystals have size-dependent optical absorbances that make detection wavelength an issue for data collection. Additionally, to obtain accurate data for nanoparticles rotor speeds should be selected to permit complete sedimentation within 6 h.

Acknowledgments

This work is supported by the Nanoscale Science and Engineering Initiative of the National Science Foundation under NSF Award Number EEC-0647452 and the Robert A Welch Foundation (C-1342). JAJ was supported by a training fellowship from the W M Keck Foundation to the Gulf Coast Consortia (NIH Grant No. 1 T90 DK70121-01 and 1 R90 DK71504-01).

References

[1] Calabretta M, Jamison J A, Falkner J C, Liu Y, Yuhas B D, Matthews K S and Colvin V L 2005 Analytical ultracentrifugation for characterizing nanocrystals and their bioconjugates *Nano Lett.* **5** 963–7

[2] Colfen H, Tirosh S and Zaban A 2003 Nanocrystal surface structure analysis by analytical ultracentrifugation *Langmuir* **19** 10654–9

[3] Niederberger M, Garnweiter G, Krumeich F, Nesper R, Colfen H and Antonietti M 2004 Tailoring the surface and solubility properties of nanocrystalline titania by a nonaqueous *in situ* functionalization process *Chem. Mater.* **16** 1202–8

[4] Nichols J B, Kraemer E O and Bailey E D 1932 The particle size and constitution of colloidal ferric oxide *J. Phys. Chem.* **36** 326–39

[5] Pinna N, Grancharov S, Beato P, Bonville P, Antonietti M and Niederberger M 2005 Magnetite nanocrystals: nonaqueous synthesis, characterization, and solubility *Chem. Mater.* **17** 3044–9

[6] Bronstein L, Sidorov S N, Valetsky P M, Hartmann J, Colfen H and Antonietti M 1999 Induced micellization by interaction of poly(2-vinylpyridine)-block-poly(ethylene oxide) with metal compounds. Micelle characteristics and metal nanoparticle formation *Langmuir* **15** 6256–62

[7] Colfen H, Schnablegger H, Fisher A, Jentoft F C, Weinberg G and Schlogl R 2002 Particle growth kinetics in zirconium sulfate aqueous solutions followed by dynamic light scattering and analytical ultracentrifugation: implications for thin film deposition *Langmuir* **18** 3500–9

[8] Svedberg E B, Ahner J, Sukla N, Ehrman S H and Schilling K 2005 FePt nanoparticle hydrodynamic size and densities form the polyol process as determined by analytical ultracentrifugation *Nanotechnology* **16** 953–6

[9] Bootz A, Vogel V, Schubert D and Kreuter J 2004 Comparison of scanning electron microscopy, dynamic light scattering and analytical ultracentrifugation for the sizing of poly(butylcyanoacrylate) nanoparticles *Eur. J. Pharm. Biopharm.* **57** 369–75

[10] Bronstein L, Chernyshov D M, Timofeeva G I, Dubrovina L V, Valetsky P M, Obolonkova E S and Khokhlov A R 2000 Interaction of polystyrene-block-poly(ethylene oxide) micelles with cationic surfactant in aqueous solutions. Metal colloid formation in hybrid systems *Langmuir* **16** 3626–32

[11] Bronstein L M *et al* 2006 Morphology of hybrid poly styrene-block-poly(ethylene oxide) micelles: analytical ultracentrifugation and sans studies *J. Colloid Interface Sci.* **299** 944–52

[12] Colfen H, Volkel A, Shinichi E, Kobold U, Kaufmann J, Puhlmann A, Goltner C and Wachernig H 2002 Mechanism of nanoparticle-enhanced turbidimetric assays applying nanoparticles of different size and immunoreactivity *Langmuir* **18** 7623–8

[13] Colfen H 2004 Analytical ultracentrifugation of nanoparticles *Polym. News* **29** 101–16

[14] Colfen H 2004 Analysis of nanoparticles <10 nm by analytical ultracentrifugation *ACS Symposium Series* vol 881 pp 119–37

[15] Colfen H and Pauck T 1997 Determination of particle size distributions with angstrom resolution *Colloid Polym. Sci.* **275** 175–80

[16] Deshpande A S, Pinna N, Beato P, Antonietti M and Niederberger M 2004 Synthesis and characterization of stable and crystalline $Ce(1-x)Zrx$O2 nanoparticle sols *Chem. Mater.* **16** 2599–604

[17] Gittins D I and Caruso F 2001 Tailoring the polyelectrolyte coating of metal nanoparticles *J. Phys. Chem.* B **105** 6846–52

[18] Gohon Y, Giusti F, Prata C, Charvolin D, Timmins P, Ebel C, Tribet C and Popot J L 2006 Well-defined nanoparticles formed by hydrophobic assembly of a short and polydisperse random terpolymer, amphipol A8-35 *Langmuir* **22** 1281–90

[19] Joralemon M J, Murthy K S, Remsen E E, Becker M L and Wooley K L 2004 Synthesis, characterization, and bioavailability of mannosylated shell cross-linked nanoparticles *Biomacromolecules* **5** 903–13

[20] Joralemon M J, Smith N L, Holowka D, Baird B and Wooley K L 2005 Antigen-decorated shell cross-linked nanoparticles: synthesis, characterization, and antibody interactions *Bioconjug. Chem.* **16** 1246–56

[21] Joralemon M J, O'Reilly R K, Hawker C J and Wooley K L 2005 Shell click-crosslinked (Scc) nanoparticles: a new methodology for synthesis and orthogonal functionalization *J. Am. Chem. Soc.* **127** 16892–99

[22] Lechner M D and Machtle W 1999 Characterization of nanoparticles *Macromol. Symp.* **145** 1–7

[23] Lechner M D and Machtle W 2000 Characterization of nanoparticles *Trends in Advanced Materials and Processes* vol 352 (Zurich-Uetikon: Trans Tech Publications) pp 87–90

[24] Machtle W 1999 High-resolution, submicron particle size distribution analysis using gravitational-sweep sedimentation *Biophys. J.* **76** 1080–91

[25] Machtle W and Borger L 2006 *Analytical Ultracentrifugation of Polymers and Nanoparticles* 1st edn (Berlin: Springer)

[26] Mayya K S, Schoeler B and Caruso F 2003 Preparation and organization of nanoscale polyelectrolyte-coated gold nanoparticles *Adv. Funct. Mater.* **13** 183–8

[27] Mayya K S and Caruso F 2003 Phase transfer of surface-modified gold nanoparticles by hydrophobization with alkylamines *Langmuir* **19** 6987–93

[28] Rapoport D H, Vogel W, Colfen H and Schlogl R 1997 Ligand-stabilized metal clusters: reinvestigation of the structure of $Au_{55}[P(C_6H_5)_3]_{12}Cl_6$ *J. Phys. Chem.* B **101** 4175–83

[29] Remsen E E, Thurmond K B II and Wooley K L 1999 Solution and surface charge properties of shell cross-linked Knedel nanoparticles *Macromolecules* **32** 3685–9

[30] Sokolova V, Prymak O, Meyer-Zaika W, Colfen H, Rehage H, Shukla A and Epple M 2006 Synthesis and characterization of DNA-functionalized calcium phosphate nanoparticles *Mater.wiss. Werkst.tech.* **37** 441–5

[31] ThiesWeesie D M E, Philipse A P and Lekkerkerker H N W 1996 Sedimentation of bidisperse, uncharged colloidal sphere suspensions: influence of viscosity and irregular surfaces *J. Colloid Interface Sci.* **177** 427–38

[32] ThiesWeesie D M E, Philipse A P, Nagele G, Mandl B and Klein R 1995 Nonanalytical concentration-dependence of sedimentation of charged silica spheres in an organic-solvent—experiments and calculations *J. Colloid Interface Sci.* **176** 43–54

[33] Tziatos C, Precup A A, Weidl C H, Schubert U S, Schuck P, Durchschlag H, Machtle W, van den Broek J A and Schubert D 2002 Studies on the partial specific volume of a poly(ethylene glycol) derivative in different solvent systems *Prog. Colloid Polym. Sci.* **119** 24–30

[34] Vogel V, Langer K, Balthasar S, Schuck P, Machtle W, Haase W, van den Broek J A, Tziatzios C and Schubert D 2002 Characterization of serum albumin nanoparticles by sedimentation velocity analysis and electron microscopy *Prog. Colloid Polym. Sci.* **119** 31–6

[35] Vogel V, Gohy J-F, Lohnmeijer B G G, van der Broek J A, Haase W, Schubert U S and Schubert D 2003 Metallo-supramolecular micelles: studies by analytical ultracentrifugation and electron microscopy *J. Polym. Sci.* A **41** 3159–68

[36] Vogel V *et al* 2005 Oligonucleotide-protamine-albumin nanoparticles: preparation, physical properties, and intracellular distribution *J. Control. Release* **103** 99–111

[37] Wang H and Wen C S 1999 Concentration-dependent sedimentation of stable magnetic dispersions *J. Colloid Interface Sci.* **213** 606–8

[38] Arnold M S, Suntivich J, Stupp S I and Hersam M C 2008 Hydrodynamic characterization of surfactant encapsulated carbon nanotubes using an analytical ultracentrifuge *ACS Nano* **2** 2291–300

[39] Liu T, Luo S D, Xiao Z W, Zhang C and Wang B 2008 Preparative ultracentrifuge method for characterization of carbon nanotube dispersions *J. Phys. Chem.* C **112** 19193–202

[40] Lange H 1995 Comparative test of methods to determine particle-size and particle-size distribution in the submicron range *Part. Part. Syst. Charact.* **12** 148–57

[41] Jamison J A, Krueger K M, Yavuz C T, Mayo J T, Lecrone D, Redden J J and Colvin V L 2008 Size-dependent sedimentation properties of nanocrystals *ACS Nano* **2** 311–9

[42] Svedberg T and Nichols J B 1923 Determination of size and distribution of size of particles by centrifugal methods *J. Am. Chem. Soc.* **45** 2910–7

[43] Yu W W and Peng X G 2002 Formation of high-quality CdS and other II-VI semiconductor nanocrystals in noncoordinating solvents: tunable reactivity of monomers *Angew. Chem.* **41** 2368–71

[44] Krueger K M, Al-Somali A M, Falkner J C and Colvin V L 2005 Characterization of nanocrystalline CdSe by size exclusion chromatography *Anal. Chem.* **77** 3511–5

[45] Yu W W, Qu L, Guo W and Peng X 2003 Experimental determination of the extinction coefficient of CdTe, CdSe, and CdS nanocrystals *Chem. Mater.* **15** 2854–60

[46] Yavuz C T *et al* 2006 Low-field magnetic separation of monodisperse Fe_3O_4 nanocrystals *Science* **314** 964–7

[47] Schuck P 2000 Size-distribution analysis of macromolecules by sedimentation velocity ultracentrifugation and Lamm equation modeling *Biophys. J.* **78** 1606–19

[48] Schuck P and Rossmanith P 2000 Determination of the sedimentation coefficient distribution G*(S) by least-squares boundary modeling *Biopolymers* **54** 328–41
[49] Lechner M D and Machtle W 1999 Determination of the particle size distribution of 5–100 nm nanoparticles with the analytical ultracentrifuge: consideration and correction of diffusion effects *Prog. Colloid Polym. Sci.* **113** 37–43
[50] Leibowitz J, Lewis M S and Schuck P 2002 Modern analytical ultracentrifugation in protein science: a tutorial review *Protein Sci.* **11** 2067–79
[51] Demeler B, Saber H and Hansen J C 1997 Identification and interpretation of complexity in sedimentation velocity boundaries *Biophys. J.* **72** 397–407
[52] van Holde K E and Weischet W O 1978 Boundary analysis of sedimentation velocity experiments with monodisperse and paucidisperse solutes *Biopolymers* **17** 1387–403
[53] Sood S M and Slattery C W 2001 Association of mixtures of the two major forms of beta-casein from human milk *J. Dairy Sci.* **84** 2163–9
[54] Cole J L 1996 Characterization of human cytomegalovirus protease dimerization by analytical centrifugation *Biochemistry* **35** 15601–10
[55] Lavrenko P, Okatova O, Korneeva E and Finkelmann H 1999 Temperature effects in hydrodynamic properties of comb-like polymer with laterally attached mesogenic units *Polymer* **40** 1701–7
[56] Hahn M, Gornitz E and Dautzenberg H 1998 Synthesis and properties of ionically modified polymers with Lcst behavior *Macromolecules* **31** 5616–23
[57] Colfen H, Harding S E, Wilson E K, Scrutton N S and Winzor D J 1997 Low temperature solution behaviour of methylophilus methylotrophus electron transferring flavoprotein: a study by analytical ultracentrifugation *Eur. Biophys. J.* **25** 411–6
[58] Colfen H, Harding S E, Wilson E K, Packman L C and Scrutton N S 1996 Homodimeric and expanded behaviour of trimethylamine dehydrogenase in solution at different temperatures *Eur. Biophys. J.* **24** 159–64
[59] Beck K, Gambee J E, Bohan C A and Bachinger H P 1996 The C-terminal domain of cartilage matrix protein assembles into a triple-stranded alpha-helical coiled-coil structure *J. Mol. Biol.* **256** 909–23
[60] Pathmamanoharan C and Philipse A P 1998 Preparation and properties of monodisperse magnetic cobalt colloids grafted with polyisobutene *J. Colloid Interface Sci.* **205** 340–53
[61] van der Kooij F M, Philipse A P and Dhont J K G 2000 Sedimentation and diffusion in suspensions of sterically stabilized colloidal platelets *Langmuir* **16** 5317–23
[62] Dogic Z, Philipse A P, Fraden S and Dhont J K G 2000 Concentration-dependent sedimentation of colloidal rods *J. Chem. Phys.* **113** 8368–80
[63] Donselaar L N and Philipse A P 1999 Interactions between silica colloids with magnetite cares: diffusion, sedimentation and light scattering *J. Colloid Interface Sci.* **212** 14–23
[64] Donselaar L N, Philipse A P and Suurmond J 1997 Concentration-dependent sedimentation of dilute magnetic fluids and magnetic silica dispersions *Langmuir* **13** 6018–25
[65] Schulte C, Morrison C A and Garrett R A 1974 Ribosomal proteins. 76. protein-ribonucleic acid interactions in *Escherichia coli* ribosomes. Solution studies on S4-16s ribonucleic acid and L24-23s ribonucleic acid binding *Biochemistry* **13** 1032–7
[66] Stowell C and Korgel B A 2001 Self-assembled honeycomb networks of gold nanocrystals *Nano Lett.* **1** 595–600
[67] Lisiecki I, Albouy P A and Pileni M P 2004 'Supra' crystal: control of the ordering of self-organization of cobalt nanocrystals at the mesoscopic scale *J. Phys. Chem.* B **108** 20050–5